begell house, inc.
Journal Production
50 Cross Highway
Redding, CT 06896
Phone: 1-203-938-1300
Fax: 1-203-938-1304
Begell House Production Contact : journals@begellhouse.com

Dear Corresponding Author,

Effective April 2011 Begell House will no longer provide corresponding authors with a print copy of the issue in which their article appears. Corresponding authors will now receive a pdf file of the final version of their article that has been accepted for publication.

Please note that the pdf file provided is for your own personal use and is not to be posted on any websites or distributed in any manner (electronic or print). Please follow all guidelines provided in the copyright agreement that was signed and included with your original manuscript files.

Any questions or concerns pertaining to this matter should be addressed to journals@begellhouse.com

Thank you for your contribution to our journal and we look forward to working with you again in the future.

.

Sincerely,

Michelle Amoroso

Michelle Amoroso
Production Department

Journal of Porous Media, 15 (10): 957–973 (2012)

DEVELOPMENT OF DIMENSIONLESS NUMBERS FOR HEAT TRANSFER IN POROUS MEDIA USING A MEMORY CONCEPT

M. Enamul Hossain & Sidqi A. Abu-Khamsin*

Department of Petroleum Engineering, King Fahd University of Petroleum & Minerals, Dhahran 31261, Kingdom of Saudi Arabia

*Address all correspondence to M. Enamul Hossain E-mail: menamul@kfupm.edu.sa

Original Manuscript Submitted: 11/29/2010; Final Draft Received: 5/2/2011

Various dimensionless numbers such as the Nusselt, Prandtl, and Peclet numbers, play a significant role in the analysis of heat transfer in any non-isothermal physical system. This transport phenomenon is modeled by a very complex set of differential equations that could involve a large number of variables and for which analytical solutions may be unattainable. Therefore, the model equations are often linearized by neglecting one or more terms (such as convection) or by employing simplifying assumptions. With the advent of advanced computational tools, it is possible to tackle such mathematical challenges numerically. Using a mathematical model based on nonlinear energy balance equations, new dimensionless numbers were developed to describe the role of various heat transport mechanisms (such as conduction and convection) in thermal recovery processes in porous media. The results show that the proposed numbers are sensitive to most of the reservoir rock/fluid properties such as porosity, permeability, densities, heat capacities, etc. Therefore, the proposed dimensionless numbers help to characterize the rheological behavior of the rock–fluid system. This work will enhance the understanding of the effect of heat transfer on the alteration of effective permeability during thermal recovery operations in a hydrocarbon reservoir.

KEY WORDS: *heat transfer, porous media, dimensionless number, temperature distribution, temperature profile, numerical simulation, reservoir management*

1. INTRODUCTION

The analysis of the temperature distribution in a reservoir formation is gaining importance due to its utility in detecting water or gas influx entering into the wellbore. It is also a key factor in evaluating the performance of thermal recovery processes such as hot water injection, steam flooding, and in situ combustion. The temperature distribution is governed mainly by heat transfer within the rock matrix and its fluid content, which is controlled by the highly complex characteristics of the rock/fluid interaction. Furthermore, heat transfer depends on the fluid temperature, which is related to the surrounding temperature, surrounding conductivity (e.g., limestone, sea water, and air), insulation, intra-film conductivity, and residence time.

Recent advances in pressure and temperature measurement within porous media have enabled researchers to investigate temperature propagation patterns and their dependence on various parameters during thermal operations (Dawkrajai et al., 2006; Yoshioka et al., 2006; Hossain et al., 2008a, 2009a), who concluded that the temperature distribution is much more sensitive to time and formation fluid velocity. It is also sensitive to the steam or hot water injection rate or velocity. Researchers have assumed a linear function for fluid velocity in the formation but did not consider the thermal effects in terms of the Nusselt, Peclet, and Prandtl numbers.

The alteration of rock/fluid properties during thermal processes are well established in the literature, mainly by Hossain and co-workers (Hossain et al., 2007, 2008a, 2009a; Hossain and Islam, 2009). Such alterations of

1091–028X/12/$35.00

NOMENCLATURE

API	American petroleum institute
c_f	total fluid compressibility (1/Pa)
c_s	reservoir formation rock compressibility (1/Pa)
c_t	total compressibility (1/Pa)
c_{pf}	specific heat capacity of reservoir fluid (kJ/kg K)
c_{pg}	specific heat capacity of injected hot water (kJ/kg K)
c_{po}	specific heat capacity of reservoir oil (kJ/kg K)
c_{ps}	specific heat capacity of reservoir rock (kJ/kg K)
c_{pw}	specific heat capacity of water (kJ/kg K)
D	diameter (m)
g	gravitational acceleration in x direction (m/s^2)
h_c	convection heat transfer coefficient (kJ/hm^2 K)
k	absolute permeability of solid rock matrix (m^2)
k_i	initial permeability of solid rock matrix (m^2)
k_f	thermal conductivity of reservoir fluid (kJ/hm K)
k_g	thermal reservoir gas (kJ/hm K)
k_o	thermal conductivity of reservoir oil (kJ/hm K)
k_s	thermal conductivity of reservoir rock (kJ/hm K)
k_w	thermal conductivity of water (kJ/hm K)
k_e	effective thermal conductivity of solid rock matrix (kJ/hm K)
K_{mc}	mass transfer coefficient (m/s)
L	distance between injection and production wells along x direction (m)
L_c	characteristic length ($2\pi r_{pt}$) (i.e., pore throat diameter of the porous rock matrix) (m)
$L_{c-\mathrm{Bi}}$	characteristic length for Biot number ($V_{\mathrm{body}}/A_{\mathrm{surface}}$) (m)
$L_{c-\mathrm{Bo}}$	characteristic length for Bond number (m)
$L_{c-\mathrm{Fo}}$	characteristic length for Fourier number (m)
$L_{c-\mathrm{Gr}}$	characteristic length for Grashof number (m)
$L_{c-\mathrm{Nu}}$	characteristic length for Nusselt number (m)
$L_{c-\mathrm{Pe}}$	characteristic length for Peclet number (m)
$L_{c-\mathrm{Ra}}$	characteristic length for Rayleigh number (m)
$L_{c-\mathrm{Re}}$	characteristic length for Reynolds number (m)
$L_{c-\mathrm{Sh}}$	characteristic length for Sherwood number (m)
$L_{c-\mathrm{We}}$	characteristic length for Weber number (m)
L^*	dimensionless length of the reservoir
M	average system heat capacity (kJ/m^3 K)
N	rotational speed (rpm)
$N_{\mathrm{Nu}L}$	local Nusselt number, dimensionless ($h_c L_c/k_e$)
$N_{\mathrm{Pe}L}$	local Peclet number, dimensionless ($L_c \rho_f c_{pf} u_x/k_e$)
N_{Pr}	Prandtl number, dimensionless ($\mu c_{pf}/k_e$)
$(N_{\mathrm{Pr}})_f$	Prandtl number of fluid in porous medium, dimensionless ($\mu c_{pf}/k_f$)
$(N_{\mathrm{Pr}})_{fs}$	Prandtl number of fluid-saturated porous medium, dimensionless (α_H/α_{Te})
$(N_{\mathrm{Pr}})_b$	bulk Prandtl number of fluid-saturated porous medium, dimensionless (ν/α_{Tb})
p	pressure of the system (Pa)
P_W	power (hp)
p_i	initial pressure of the system (Pa)
p_o	a reference pressure of the system (Pa)
q_i	initial volumetric production rate (m^3/s)
q_{inj}	volumetric injection rate of hot water (m^3/s)
q_{prod}	volumetric production rate of oil (m^3/s)
q_x	fluid mass flow rate per unit area in x-direction (kg/m^2 s)
r_{pt}	pore-throat radius (microns)
rb	reservoir barrels

NOMENCLATURE (Continued)

stb	standard barrel
scf	standard cubic feet
S_g	gas saturation (volume fraction)
S_o	oil saturation (volume fraction)
S_w	water saturation (volume fraction)
S_{wi}	initial water saturation (volume fraction)
t	time (s)
t^*	dimensionless time
t_C	characteristic time (s)
T	temperature (K)
T^*	dimensionless temperature
T_i	initial reservoir temperature (K)
T_f	reservoir fluid temperature (K)
T_r	reference temperature of injected fluid (K)
T_s	average temperature of solid rock matrix (K)
T_{st}	temperature of injected hot water (K)
u_i	initial fluid velocity along x direction (m/s)
u_x	fluid velocity along x direction at any time t (m/s)
u^*	dimensionless velocity
V	fluid velocity of the Reynolds number (m/s)
V_L	characteristic velocity of liquid (m/s)
x	flow dimension at any point along x-direction (m)
x^*	dimensionless distance respectively

Greek Symbols

α	fractional order of differentiation, dimensionless
α_H	hydraulic diffusivity of fluid-saturated porous medium ($k/\varphi\mu c_t$) (m^2/s)
α_m	mass diffusivity (m^2/s)
α_{Tb}	bulk thermal diffusivity of the fluid-saturated porous medium (k_e/M) (m^2/s)
α_{Te}	effective thermal diffusivity of fluid-saturated porous medium ($k_f/\varphi\rho_f c_{pf}$) (m^2/s)
α_{Tf}	absolute thermal diffusivity of reservoir fluid ($k_f/\rho_f c_{pf}$) (m^2/s)
α_{Ts}	absolute thermal diffusivity of solid rock matrix ($k_s/\rho_s c_{ps}$) (m^2/s)
β	volumetric thermal expansion coefficient $\left[(1/V)(\partial V/\partial p)_p\right]$ (m^3/m^3 K)
ΔT	temperature difference (K)
$\Delta\rho$	density difference of fluids (i.e., water and oil) ($\rho_w - \rho_o$) (kg/m^3)
ν	kinematic viscosity (ratio of absolute or dynamic viscosity to density) (μ/ρ_f) (m^2/s)
η	ratio of the pseudo-permeability of the medium with memory to fluid viscosity ($m^3 s^{1+\alpha}$/kg)
μ_i	initial fluid dynamic viscosity (Pa/s)
μ_L	fluid dynamic viscosity (Pa/s)
ξ	a dummy variable for time (i.e., real part in the plane of the integral) (s)
Γ	gamma function
ρ	fluid density (kg/m^3)
ϕ	porosity of the rock (volume fraction)
ϕ_i	initial porosity of rock (volume fraction)
ρ_f	density of fluid (kg/m^3)
ρ_g	density of gas (kg/m^3)
ρ_o	density of oil (kg/m^3)
ρ_s	density of solid rock (kg/m^3)
ρ_w	density of water (kg/m^3)
σ_{Bo}	surface tension of the interface or interfacial forces for Bond number (N/m)
σ_{Ca}	surface tension of the interface or interfacial forces for Capillary number (N/m)
σ_{We}	surface tension of the interface or interfacial forces for Weber number (N/m)

rock/fluid properties influence heat transfer, which governs the temperature profile within the reservoir. The literature also shows that the fluid velocity (Yoshioka et al., 2005a,b) and time (Hossain, 2008; Hossain et al., 2008a,b) have strong effects on the temperature profile. Since available models are unable to handle the alteration

of rock/fluid properties with time during a thermal operation (Marx and Langenheim, 1959; Willman et al., 1961; Spillette, 1965; Chan and Banerjee, 1981; Kaviany, 2002; Hossain et al., 2008b, 2009b), this study focuses on the development of new dimensionless numbers that characterize heat transfer while incorporating the concept of "memory." Memory is defined as the effect of past events on the present and future course of developments. In this work, it refers to the continuous alteration of the rheological behavior of a rock/fluid system with time (Hossain et al., 2009a). Therefore, it is important to investigate the effects of memory in terms of various heat transfer dimensionless numbers based on the rheology of a rock/fluid system. The rheology of a rock/fluid system is composed of continuous functions in time.

2. MODEL DESCRIPTION

A homogenous porous medium of uniform cross-sectional area along the x axis is considered. Instead of the customary use of Darcy's law to describe fluid flow in porous media, this study uses the modified Darcy's law (Hossain et al., 2008c; Hossain and Islam, 2009) to introduce the notion of fluid memory. Since the medium is homogeneous, the pressure along the x direction may initially be considered to vary according to the Darcy diffusivity equation. It is also assumed that the thermal conductivities of fluids and the rock matrix are not functions of temperature but rather constant throughout the medium. This is warranted by the initial uniform distributions of pressure and temperature throughout the reservoir. The computations are carried out for different fluid velocities. In this problem, the fluid is defined as a homogeneous mixture of injected hot water and the original reservoir fluid. The mixture's composition is constant throughout the reservoir. The medium is defined as a porous rock where its properties change with time and space.

3. MATHEMATICAL FORMULATION

To develop the new dimensionless numbers, the model equations for the temperature profile must first be derived based on the energy balance equation, which is considered as the governing equation for both rock and fluids separately. Such a derivation has been presented by Hossain et al. (2008b) in full detail and by Hossain et al. (2009b) in a summarized version. However, during the development of the model equations Hossain et al. (2008b, 2009b) did not consider the time-dependent rheological properties of the reservoir. The inclusion of time-dependent rock and fluid properties may be of significant value to petroleum engineers because production performance and management are usually laden with uncertainty.

Therefore, the concept of memory is introduced to the model equations in this article using the modified Darcy's law as the flow rate equation [Eq. (1)], which may be written for a one-dimensional (1D) system (Hossain et al. 2007, 2008c, 2009a) as

$$u = -\frac{\eta}{\Gamma(1-\alpha)} \int_0^t (t-\xi)^{-\alpha} \left[\frac{\partial^2 p}{\partial \xi \partial x}\right] \partial \xi \qquad (1)$$

Hossain et al. (2008c) defined the composite variable, η, which is a function of permeability and viscosity, for any type of reservoir as

$$\eta = \frac{k}{\mu_{ab}} (t)^{\alpha} \qquad (2a)$$

For example, Eq. (2a) can be expressed for sandstone as

$$\eta = \frac{\left[3.0\,(p/6894.76)^{-0.31} + 10.5\right] \times 10^{-12}}{\mu_{ob} e^{8.422\times 10^{-5}(p-p_b)}} (t)^{\alpha} \qquad (2b)$$

where

$$\mu_{ob} = 6.59927 \times 10^5 R_s^{-0.597627} T^{-0.941624} \times \gamma_g^{-0.555208} \mathrm{API}^{-1.487449}$$

$$p_b = -620.592 + 6.23087 \frac{R_s \gamma_o}{\gamma_g B_o^{1.38559}} + 2.89868T$$

$$B_o = B_{ob} e^{-C_o(p-p_b)}$$

$$B_{ob} = 1.122018 + 1.410 \times 10^{-6} \frac{R_s T}{\gamma_o^2}$$

$$C_o = \big(-70603.2 + 98.404R_s + 378.266T - 6102.03\gamma_g + 755.345\mathrm{API}\big)/(p + 3755.53)$$

In Eq. (2b), p is the fluid pressure at any time or location within the system. The bubble-point pressure (p_b) is the saturation pressure of the oil phase, which is the pressure below which gas begins to evolve and separate from the oil. The bubble-point pressure depends on the system's temperature as well as the oil composition, which is reflected by R_s, γ_o, and γ_g. As a result of gas separation, the oil volume would shrink progressively with pressure reduction, which is indicated by the oil formation volume factor (B_o). All units in Eq. (2b) are field units, which

are the oil formation volume factor (B_o), rb/stb; oil compressibility (C_o), psi^{-1}; oil formation volume factor at the bubble point (B_{ob}), rb/stb; oil viscosity at the bubble point (μ_{ob}), cp; oil viscosity above the bubble point (μ_{ab}), cp; solution gas oil ratio (R_s), scf/stb; crude oil temperature (T), °F; gas specific gravity (γ_g), lb$_m$/ft^3; oil specific gravity (γ_o), lb$_m$/ft^3; and oil API gravity (API), °API.

The 1D energy balance equations can be written to develop the new dimensionless numbers. The notion of the memory concept is incorporated into the energy balance using flow rate Eq. (1). Now, if we consider the system to have different rock and fluid temperatures ($T_s \neq T_f$), the conservation of energy equations for both the rock matrix and fluid can be written as follows (Hossain et al., 2008a,b, 2009b):

$$k_s \frac{\partial^2 T_s}{\partial x^2} = (1-\varphi)\,\rho_s c_{ps} \frac{\partial T_s}{\partial t} + \frac{h_c}{L}(T_s - T_f) \tag{3}$$

$$k_f \frac{\partial^2 T_f}{\partial x^2} - \rho_f c_{pf} u_x \frac{\partial T_f}{\partial x} = \varphi \rho_f c_{pf} \frac{\partial T_f}{\partial t} + \frac{h_c}{L}(T_f - T_s) \tag{4}$$

where

$$M = (1-\varphi)\,\rho_s c_{ps} + \varphi \rho_w c_{pw} S_w + \varphi \rho_o c_{po} S_o + \varphi \rho_g c_{pg} S_g \tag{5}$$

$$\rho_f c_{pf} = \rho_w c_{pw} S_w + \rho_o c_{po} S_o + \rho_g c_{pg} S_g \tag{6}$$

$$k_f = k_w S_w + k_o S_o + k_g S_g \tag{7}$$

$$k_e = \varphi k_f + (1-\varphi)\,k_s \tag{8}$$

$$\rho_f = \rho_w S_w + \rho_o S_o + \rho_g S_g \tag{9}$$

$$S_w + S_o + S_g = 1 \tag{10}$$

Equations (3) and (4) can be converted into dimensionless forms using dimensionless parameters defined as $T^* = T/T_i$, $T_S^* = T_S/T_i$, $T_f^* = T_f/T_i$, $x^* = x/L$, $p^* = p/p_i$, $q^* = q/q_i$, $t^* = kt/\varphi\mu c_t L^2$, and $\xi^* = kt/\varphi\mu c_t L^2$. The initial and boundary conditions are defined as $T_f^*(x,0) = T_s^*(x,0) = 1$, $T_f^*(0,t) = T_s^*(0,t) = T_{st}/T_i$, and $T_f^*(L,t) = T_s^*(L,t) = 1$.

Using these dimensionless parameters, the final forms of Eqs. (3) and (4) become (Hossain et al., 2011):

$$\frac{k_s}{k_e}\frac{\partial^2 T_s^*}{\partial x^{*2}} - N_{HA1} N_{\mathrm{Pr}} N_{HA2} \frac{\partial T_s^*}{\partial t^*} - N_{\mathrm{Nu}L} \times \frac{L}{L_c}\left(T_s^* - T_f^*\right) = 0 \tag{11}$$

$$\frac{k_f}{k_e}\frac{\partial^2 T_f^*}{\partial x^{*2}} - N_{\mathrm{Pe}L}\frac{L}{L_c}\frac{\partial T_f^*}{\partial x^*} - N_{\mathrm{Pr}} N_{HA1}\frac{\partial T_f^*}{\partial t^*} - N_{\mathrm{Nu}L}\frac{L}{L_c}\left(T_f^* - T_s^*\right) = 0 \tag{12}$$

where

$$N_{HA1} = \frac{k\rho_f}{\mu^2 c_t} \tag{13}$$

$$N_{HA2} = \frac{(1-\varphi)}{\varphi}\frac{\rho_s c_{ps}}{\rho_f c_{pf}} \tag{14}$$

In the Peclet number, u represents the case where the memory effect is considered. Therefore, during numerical computations u is used to find out the impact of memory, while the temperature distribution is governed by Eqs. (11) and (12). These two partial differential equations can be solved simultaneously to evaluate the effects of different rock/fluid parameters in terms of the Nusselt, Prandtl, and Peclet numbers. Equations (11) and (12) are also governed by the two proposed numbers that are called as N_{HA1} and N_{HA2} (where HA stands for Hossain–Abu-Khamsin).

4. SIGNIFICANCE OF PROPOSED DIMENSIONLESS NUMBERS

There are at least 15 dimensionless numbers associated with fluid dynamics and heat and mass transfer. Those numbers, along with the two proposed dimensionless numbers, are defined in Table 1. Manipulating Eq. (13) yields

$$N_{HA1} = \frac{k\rho_f}{\mu^2 c_t} = \frac{k}{\varphi\mu c_t}\frac{\varphi\rho_f}{\mu}\frac{c_{pf}}{k_f}\frac{k_f}{c_{pf}} = \alpha_H \frac{\varphi\rho_f c_{pf}}{k_f}\frac{k_f}{\mu c_{pf}} = \frac{\alpha_H}{\alpha_{Te}}\left(\frac{1}{N_{\mathrm{Pr}}}\right)_f \tag{15}$$

Therefore, N_{HA1}, expresses the influence of the rock matrix on the thermal and flow characteristics of the fluid. If the rock has no permeability, N_{HA1} becomes inversely proportional to the fluid's Prandtl number. This is the ratio of convection to conduction heat transfer between the porous rock matrix and the fluid saturating it. It is also the ratio of the momentum diffusivity over the thermal diffusivity. Therefore, the proposed number can be expressed as the hydraulic diffusivity over the momentum diffusivity. Finally, it can also be expressed as the ratio of the hydraulic diffusivity to the thermal diffusivity—both of the fluid-saturated porous medium within the system volume–divided by the Prandtl number of the fluid.

TABLE 1: Proposed new dimensionless numbers along with other dimensionless numbers used in heat transfer and fluid dynamics

Name	Symbol	Definition	Comments
Biot	N_{Bi}	$N_{\mathrm{Bi}} = h_c L_{c-\mathrm{Bi}}/k_s$	Ratio of conductive to convective heat transfer resistance
Bond	N_{Bo}	$N_{\mathrm{Bo}} = \Delta\rho g L^2_{c-\mathrm{Bo}}/\sigma_{\mathrm{Bo}}$	Ratio of body forces (often gravitational) to surface tension forces (i.e., interfacial forces)
Capillary	N_{Ca}	$N_{\mathrm{Ca}} = \mu_L V_L/\sigma_{Ca}$	Ratio of viscous forces to interfacial forces or surface tension
Fourier	N_{Fo}	$N_{\mathrm{Fo}} = \alpha_{Ts} t_c/L^2_{c-\mathrm{Fo}}$	Ratio of the heat conduction rate to the rate of thermal energy storage. It is also expressed as a ratio of current time to time to reach steady state
Grashof	N_{Gr}	$N_{\mathrm{Gr}} = g\beta\Delta T L^3_{c-\mathrm{Gr}}/\nu^2$	Ratio of the buoyancy to viscous force acting on a fluid. It is also a ratio of natural convection buoyancy force to viscous force
Proposed number 1	N_{HA1}	$N_{HA1} = k\rho_f/\mu^2 c_t$ = $\{N_{\mathrm{Pr}}\}_e/\{N_{\mathrm{Pr}}\}_f$	Ratio of the Prandtl number of the fluid-saturated porous medium to the Prandtl number of the fluid. A new dimensionless number for fluid-saturated rock
Proposed number 2	N_{HA2}	$N_{HA2} = (1-\varphi)/\varphi$ $\cdot\rho_s c_{ps}/\rho_f c_{pf}$	A new dimensionless number for fluid-saturated rock (= heat transfer of solid matrix/heat transfer of reservoir fluid)
Nusselt	N_{Nu}	$N_{\mathrm{Nu}} = h_c L_{c-\mathrm{Nu}}/k_e$	Ratio of convective to conductive heat transfer across (i.e., normal to) the boundary
Peclet	N_{Pe}	$N_{\mathrm{Pe}} = L_{c-\mathrm{Pe}}\rho_f c_{pf} u_x/k_e$ = $L_{c-\mathrm{Pe}} u_x/\alpha_{\mathrm{Tf}}$	Ratio of convective to diffusive heat/mass transport in a fluid
Power	N_{po}	$N_{po} = P_w/\rho N^3 D^5$	Also known as the Newton number and is a ratio of the resistance force to the inertia force
Prandtl	N_{Pr}	$N_{\mathrm{Pr}} = \nu/\alpha_{\mathrm{Tf}} = \mu c_{pf}/k_f$	Ratio of momentum diffusivity (kinematic viscosity) and thermal diffusivity; or ratio of viscous diffusion rate to thermal diffusion rate
Rayleigh	N_{Ra}	$N_{\mathrm{Ra}} = N_{\mathrm{Gr}} N_{\mathrm{Pr}}$ = $g\beta\Delta T L^3_{c-\mathrm{Ra}}/\nu\alpha_{\mathrm{Tf}}$	Ratio of buoyancy forces and the product of thermal and momentum diffusivities. Ratio of natural convective to diffusive heat/mass transport. Determines the transition to turbulence
Reynolds	N_{Re}	$N_{\mathrm{Re}} = \rho V L_{c-\mathrm{Re}}/\mu$	Ratio of inertial forces ($\rho V^2 L^2$) to viscous forces (μVL). Ratio of convective to viscous momentum transport
Schmidt	N_{Sc}	$N_{\mathrm{Sc}} = \nu/\alpha_m = \mu/\rho\alpha_m$	Ratio of momentum diffusivity (viscosity) and mass diffusivity and is used to characterize fluid flows in which there are simultaneous momentum and mass diffusion convection processes
Sherwood	N_{Sh}	$N_{\mathrm{Sh}} = K_{mc} L_{c-\mathrm{Sh}}/\alpha_m$	Ratio of convective to diffusive mass transport. Also called the mass transfer Nusselt number and is used in mass-transfer operations
Weber	N_{We}	$N_{\mathrm{We}} = \rho V^2 L_{\mathrm{c-We}}/\sigma_{\mathrm{We}}$	A measure of the relative importance of the fluid's inertia compared to its surface tension and related to the surface behavior for two-phase systems

In essence, N_{HA1} is the ratio of the Prandtl number of the fluid-saturated porous medium to the Prandtl number of the fluid itself:

$$N_{HA1} = \frac{(N_{\mathrm{Pr}})_s}{(N_{\mathrm{Pr}})_f} \tag{16}$$

Equation (14) can be expressed as

$$N_{HA2} = \frac{(1-\varphi)}{\varphi}\frac{\rho_s c_{ps}}{\rho_f c_{pf}} = \frac{\text{heat transfer of solid matrix}}{\text{heat transfer of reservoir fluid}} \tag{17}$$

Further manipulation yields

$$N_{HA2} = \frac{(1-\varphi)}{\varphi}\frac{k_s}{k_f}\frac{\alpha_{Tf}}{\alpha_{Ts}} = \frac{\text{heat conduction of solid}}{\text{heat conduction of fluid}} \times \frac{\text{absolute thermal diffusivity of fluid}}{\text{absolute thermal diffusivity of solid}} \tag{18}$$

5. RESULTS AND DISCUSSION

The MATLAB programming language was used to solve the model equations. The computations were carried out for a reservoir of L = 5000 m and all other assumed rock and fluid data are listed in Table 2. Hot water was injected through a well of 130 mm diameter; its temperature was different from that of the reservoir. The space and time steps were Δx^* = 0.01 and Δt^* = 0.00001.

Figures 1(a) and 1(b) show linear variations of N_{HA1} with permeability for different fluid velocities and total compressibilities, respectively. Equation (15) is employed to find these variations. Figure 1(a) shows that N_{HA1} increases with the increase of both the permeability and fluid density. On the other hand, N_{HA1} increases with the increase of permeability for any given total compressibility but decreases with the increase of total compressibility for a given permeability [Fig. 1(b)]. For an analogous system, if N_{HA1} is known, one can easily calculate the permeability value once the fluid density and total compressibility of the system are known. Figures 2(a) and 2(b) show the linear variation of N_{HA1} with the fluid velocity for different total compressibilities and fluid viscosities, respectively. Figure 2(a) shows that N_{HA1} increases with the increase of the fluid density for a particular compressibility value. However, N_{HA1} decreases with the total compressibility for the same fluid density; the same trend is true for the viscosity [Fig. 2(b)].

TABLE 2: Fluid and rock property values employed in numerical computations

Property (rock or fluid)
c_{pg} = 29.7263 (kJ/kg K)
c_{po} = 2.0934 (kJ/kg K)
c_{ps} = 0.8792 (kJ/kg K)
c_{pw} = 4.1868 (kJ/kg K)
h_c = 280.87 (kJ/hm^2 K)
k_g = 0.0143 (kJ/hm K)
k_o = 1.3962 (kJ/hm K)
k_s = 9.3460 (kJ/hm K)
k_w = 3.7758 (kJ/hm K)
k_i = 10^{-15} (m^2)
p_i = 48263299.0 (Pa)
c_f = 12.473 $\times$ 10^{-10} (1/Pa)
c_s = 5.80147 $\times$ 10^{-10} (1/Pa)
S_g = 20% (vol/vol)
S_o = 60% (vol/vol)
S_w = 20% (vol/vol)
T_{st} = 550 K
T_i = 300 K
ρ_g = 16.7121 (kg/m^3)
ρ_o = 800.923 (kg/m^3)
ρ_s = 2675.08 (kg/m^3)
ρ_w = 1000.0 (kg/m^3)
φ_i= 25% (m^3/m^3)
μ_f = 10 Pa/s (Ns/m^2)
q_i = 17.5 m^3/d (110 bbl/day)
A = 300 $\times$ 20 m = 6000 m^2

Figures 3(a)–3(c) show the nonlinear variations of N_{HA1} with the total compressibility for different permeabilities, fluid densities, and viscosities, respectively. The N_{HA1} decreases with the increase in compressibility for a particular permeability, and the nonlinearity of N_{HA1} increases with the increase in permeability [Fig. 3(a)]. For the same compressibility, N_{HA1} increases with the increase in permeability and there is no significant change of N_{HA1} when the permeability decreases to 10^{-14} m^2 (10 mD). The same trend is observed in Fig. 3(b), except that there is a fluid density effect on N_{HA1} (even if it is low). Figure 3(c) shows that low-viscosity fluids have greater effects on N_{HA1} than more viscous fluids. For the

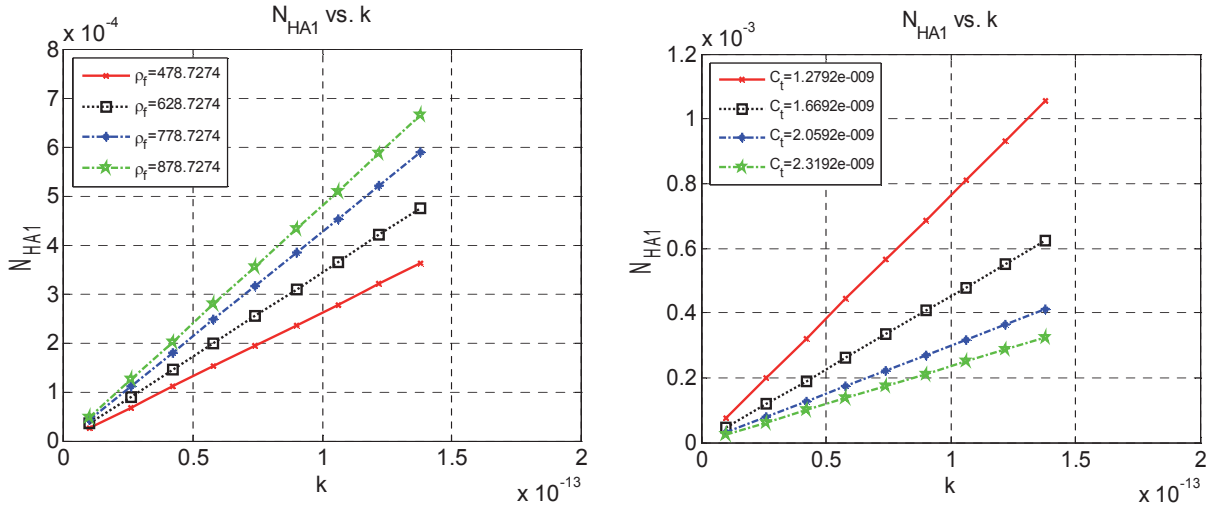

(a) (b)

FIG. 1: Variation of (N_{HA1}) with permeability (k) for different fluid viscosities (ρ_f) and total compressibilities (c_t)

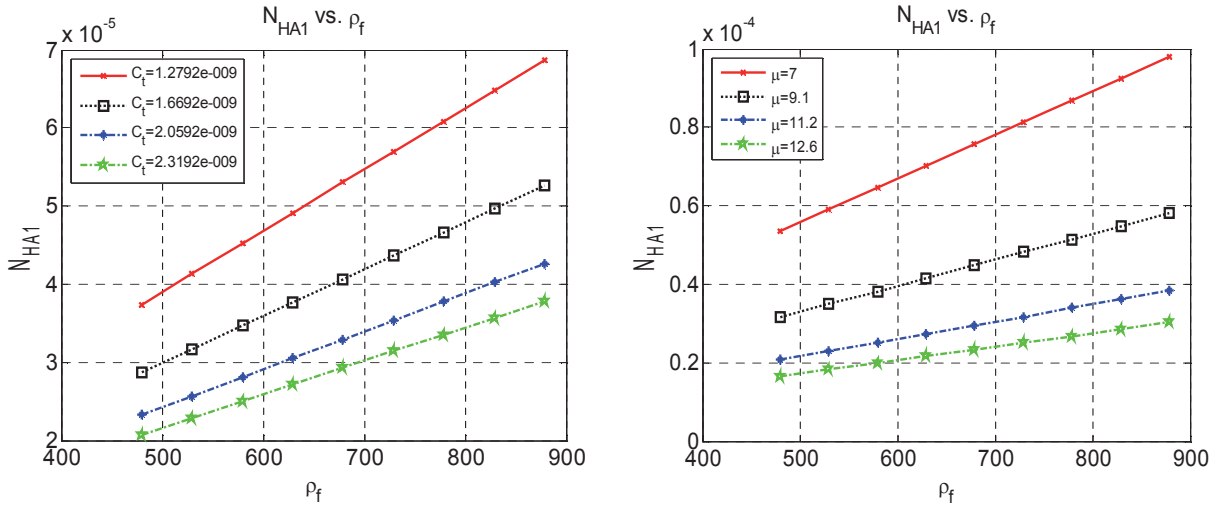

(a) (b)

FIG. 2: Variation of (N_{HA1}) with fluid density (ρ_f) for different total compressibilities (c_t), and fluid viscosities (μ)

same total compressibility, N_{HA1} decreases as the viscosity increases, which is an opposite trend to that of the permeability and fluid density.

Figures 4(a) and 4(b) depict the nonlinear variations of N_{HA1} with the fluid viscosity for different permeabilities and fluid densities, respectively. The trend of N_{HA1} variation is similar to that of Fig. 3. However, N_{HA1} is more sensitive to viscosity for different permeabilities and fluid densities compared with Fig. 3. On the other hand, the fluid density (as a result, compressibility) has more influence on N_{HA1} for low-viscosity fluids [Fig. 4(b)]. The same trend and characteristics are observed with permeability alteration on a wider range once viscosity is changed [Fig. 4(a)].

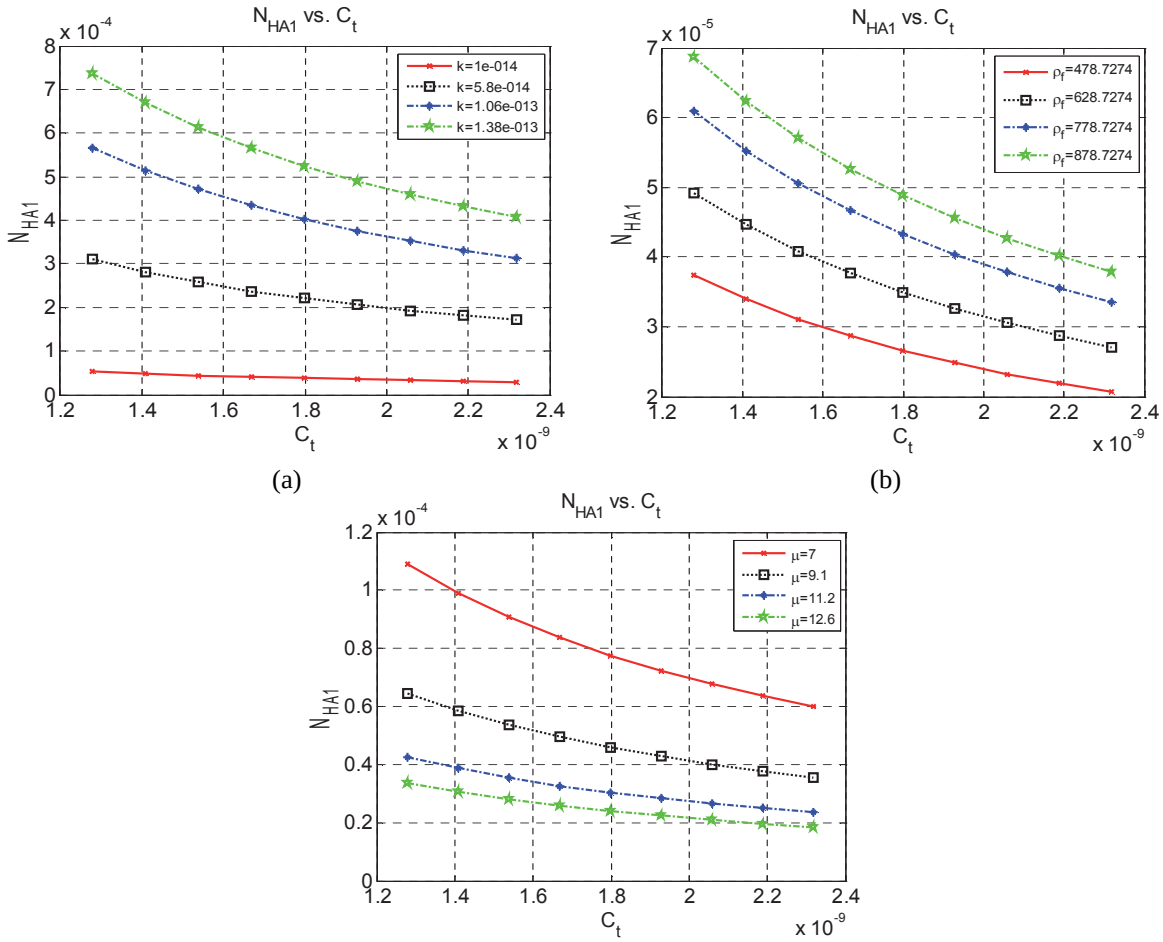

FIG. 3: Variation of (N_{HA1}) with total compressibility (c_t) for different permeabilities (k), fluid densities (ρ_f), and fluid viscosities (μ)

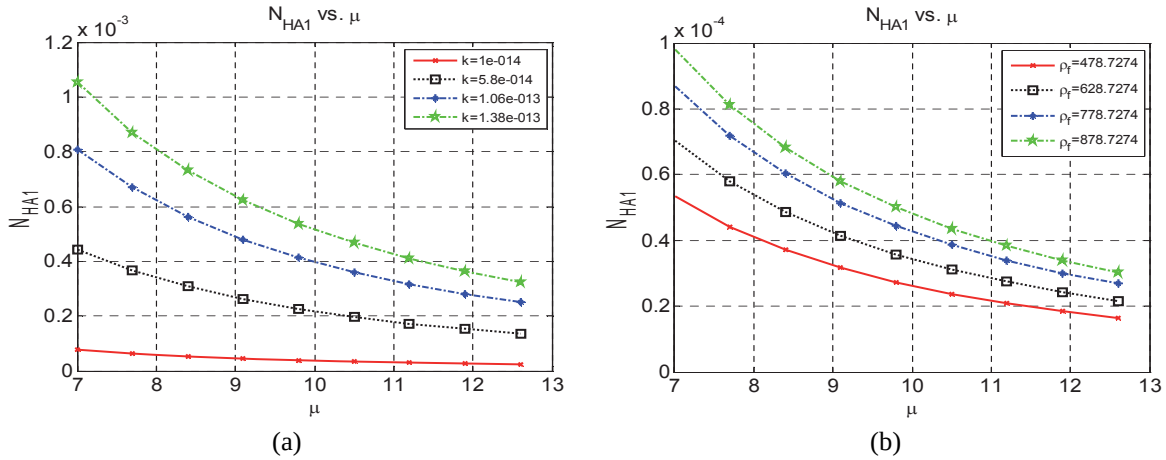

FIG. 4: Variation of (N_{HA1}) with fluid viscosity (μ) for different permeabilities (k) and fluid densities (ρ_f)

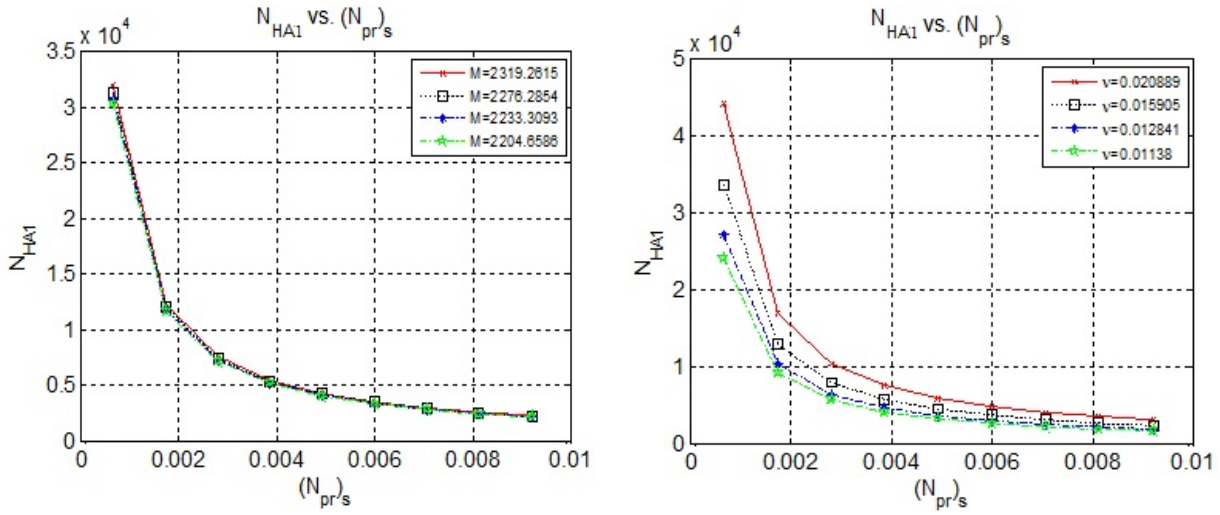

(a) (b)

FIG. 5: Variation of (N_{HA1}) with different Prandtl numbers of fluid saturated porous media [$(N_{\rm Pr})_s$]

Figures 5(a) and 5(b) show the nonlinear variations of N_{HA1} with different Prandtl numbers of the fluid-saturated porous medium $(N_{\rm Pr})_s$ for different M and ν, respectively. Initially, N_{HA1} decreases sharply for low $(N_{\rm Pr})_s$ and then gradually decreases for a given M value [Fig. 5(a)]; N_{HA1} does not change significantly with changes in M. The same trend is observed in Fig. 5(b). However, N_{HA1} increases with the increase of dynamic viscosity and the difference is significant when $(N_{\rm Pr})_s$ is below 0.002 and there is no effect of the thermal conductivity of fluid (k_f) on N_{HA1}.

Figures 6(a)–6(f) show the nonlinear decreasing trends for N_{HA2} with porosity for different ρ_s, ρ_f, c_{ps}, c_{pf}, $\rho_s c_{ps}$, and $\rho_f c_{pf}$. The decrease is initially rapid at low porosity then gradually levels off for all parameters except c_{pf} [Fig. 6(d)], where such a trend is seen for low c_{pf} values only. For high c_{pf} values, N_{HA2} approaches zero at high porosities. For the same porosity value, N_{HA2} increases with the increase of ρ_s, c_{ps}, and $\rho_s c_{ps}$ [Figs. 6(a), 6(c), and 6(e)]. On the other hand, N_{HA2} decreases with the increase of ρ_f, c_{pf}, and $\rho_f c_{pf}$ [Figs. 6(b), 6(d), and 6(f)].

Figures 7(a)–7(d) show the linear variations of N_{HA2} with the rock density for different φ, ρ_f, c_{pf}, and $\rho_f c_{pf}$. At low porosities, the slope is larger than at high porosities, but for a particular rock density N_{HA2} decreases with the increase of porosity [Fig. 7(a)]. The same trend and behavior are seen in all other figures in Fig. 7 except Fig. 7(c), where the slope markedly large only for low c_{pf} values.

Figures 8(a)–8(d) depict variations of N_{HA2} with the specific heat capacity of solid (c_{ps}) for different φ, c_{pf}, $\rho_s c_{ps}$, and ρ_s with increasing linear trends. The same behavior is shown for those rock/fluid properties as seen in Figs. 7(a)–7(d). However, when ρ_s increases, N_{HA2} increases for the same c_{ps} [Fig. 8(d)].

Figures 9(a)–9(d) depict variations of N_{HA2} with fluid density (ρ_f) for different φ, c_{pf}, c_{ps}, and $\rho_s c_{ps}$ with a nonlinear decreasing trend. As φ and c_{pf} decrease, N_{HA2} increases. However, the slopes of the N_{HA2} versus ρ_f plots for high φ and c_{pf} decrease faster than for low φ and c_{pf} [Figs. 9(a) and 9(b)]. For the same ρ_f, N_{HA2} decreases with the increase of φ and c_{pf}. On the other hand, the slopes of N_{HA2} versus ρ_f plots continue to decrease for c_{ps} and $\rho_s c_{ps}$ in a moderate way [Figs. 9(c) and 9(d)]. However, for the same ρ_f, N_{HA2} increases with the increase of c_{ps} and $\rho_s c_{ps}$. Figures 10(a)–10(d) depict N_{HA2} versus the specific heat capacity of the fluid (c_{pf}) for different φ, ρ_s, c_{ps}, and $\rho_s c_{ps}$ with decreasing nonlinear trends. For all four parameters, a sharp decrease in N_{HA2} is observed up to a c_{pf} value of 7, then it switches to a gentler decline beyond a value of 10. However, for the same value of c_{pf}, N_{HA2} decreases with the increase of φ and increases with the increase of ρ_s, c_{ps}, and $\rho_s c_{ps}$.

Figures 11(a)–11(d) depict N_{HA2} versus $\rho_f c_{pf}$ for different φ, ρ_s, c_{ps}, and $\rho_s c_{ps}$ with decreasing nonlinear

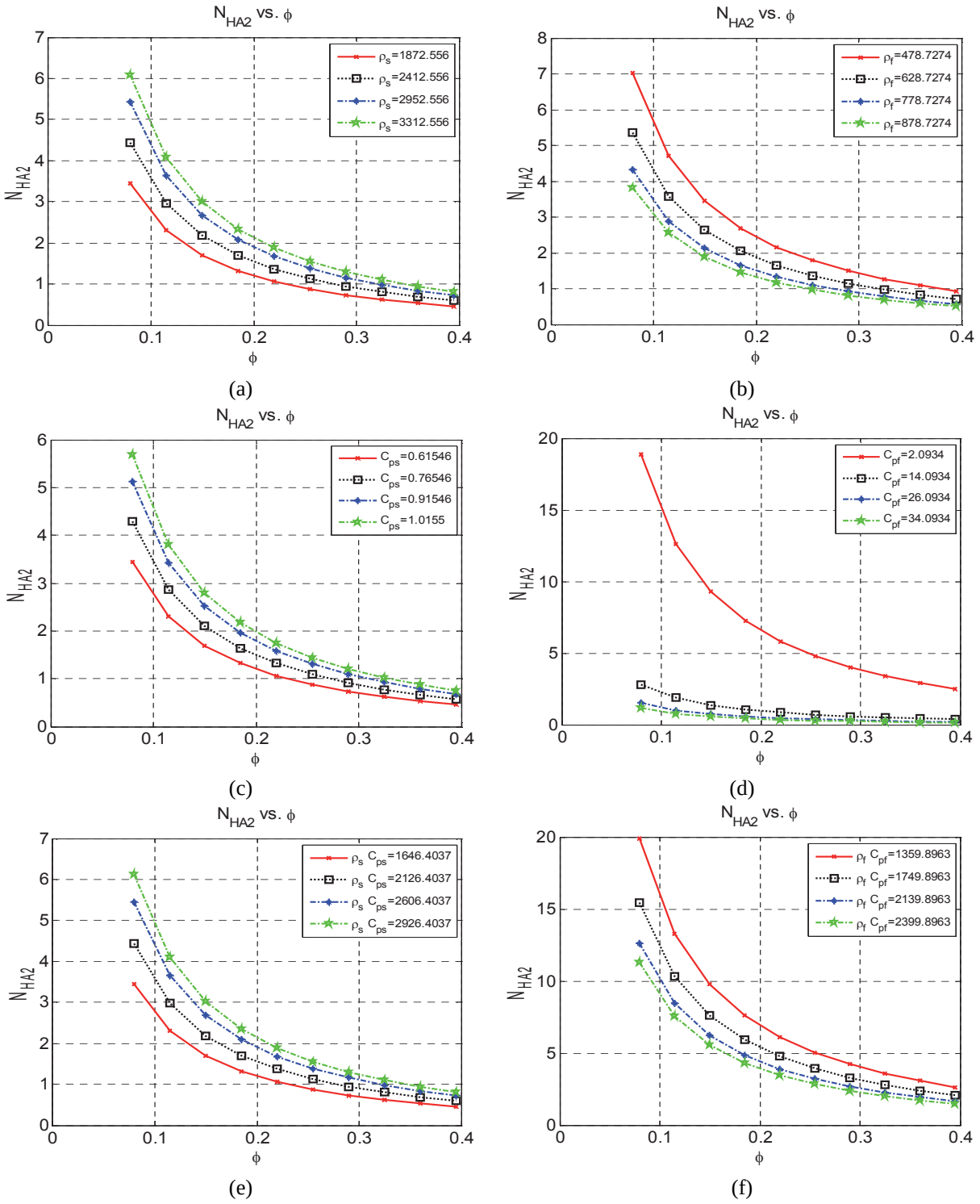

FIG. 6: Variation of (N_{HA2}) with porosity (φ) for different rock densities (ρ_s), fluid densities (ρ_f), specific heat capacities of solid (c_{ps}), specific heat capacities of fluid (c_{pf}), and different ($\rho_s c_{ps}$) and ($\rho_f c_{pf}$)

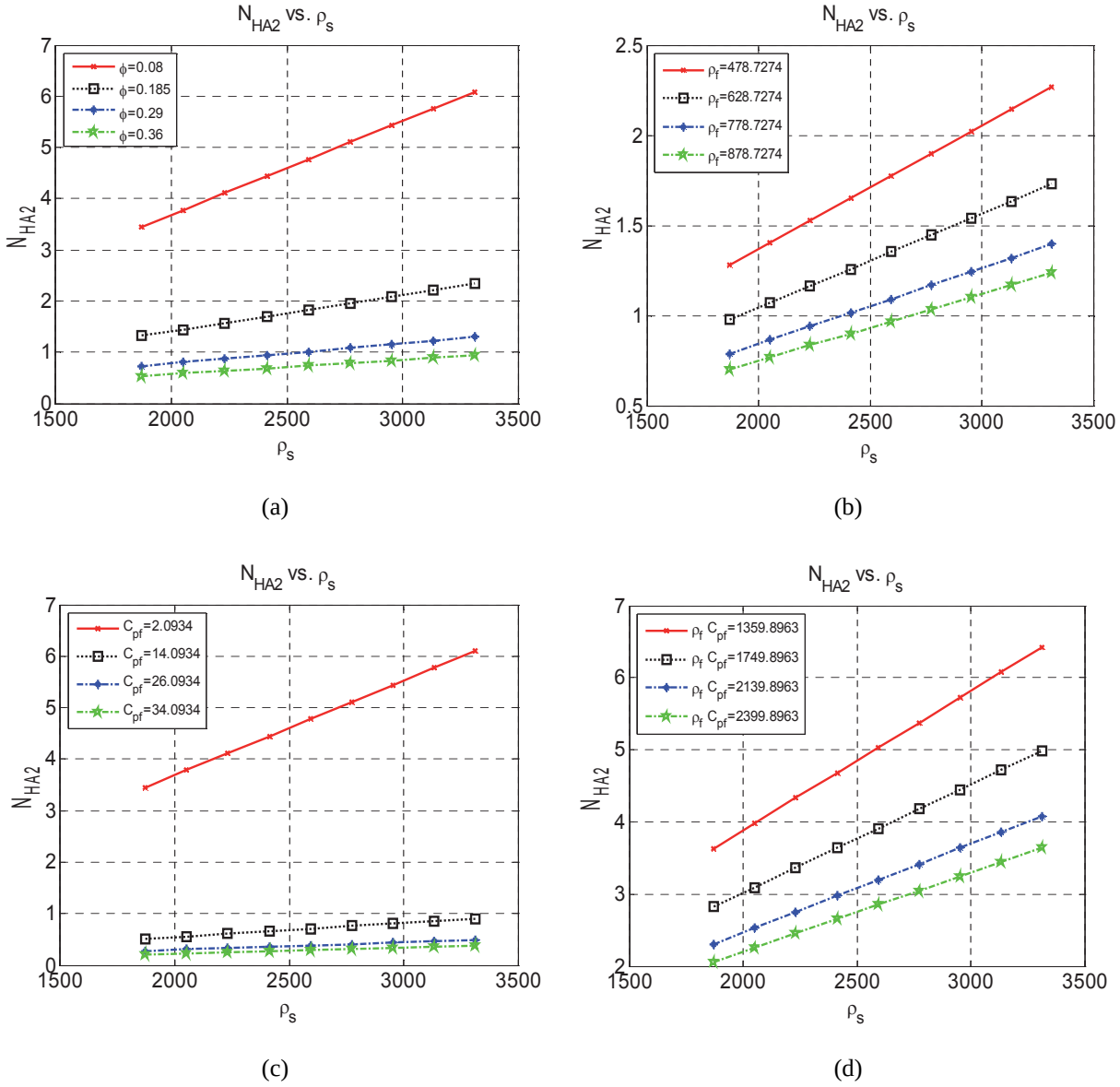

FIG. 7: Variation of (N_{HA2}) with rock density (ρ_s) for different porosities (φ), fluid densities (ρ_f), specific heat capacities of fluid (c_{pf}) and ($\rho_f c_{pf}$)

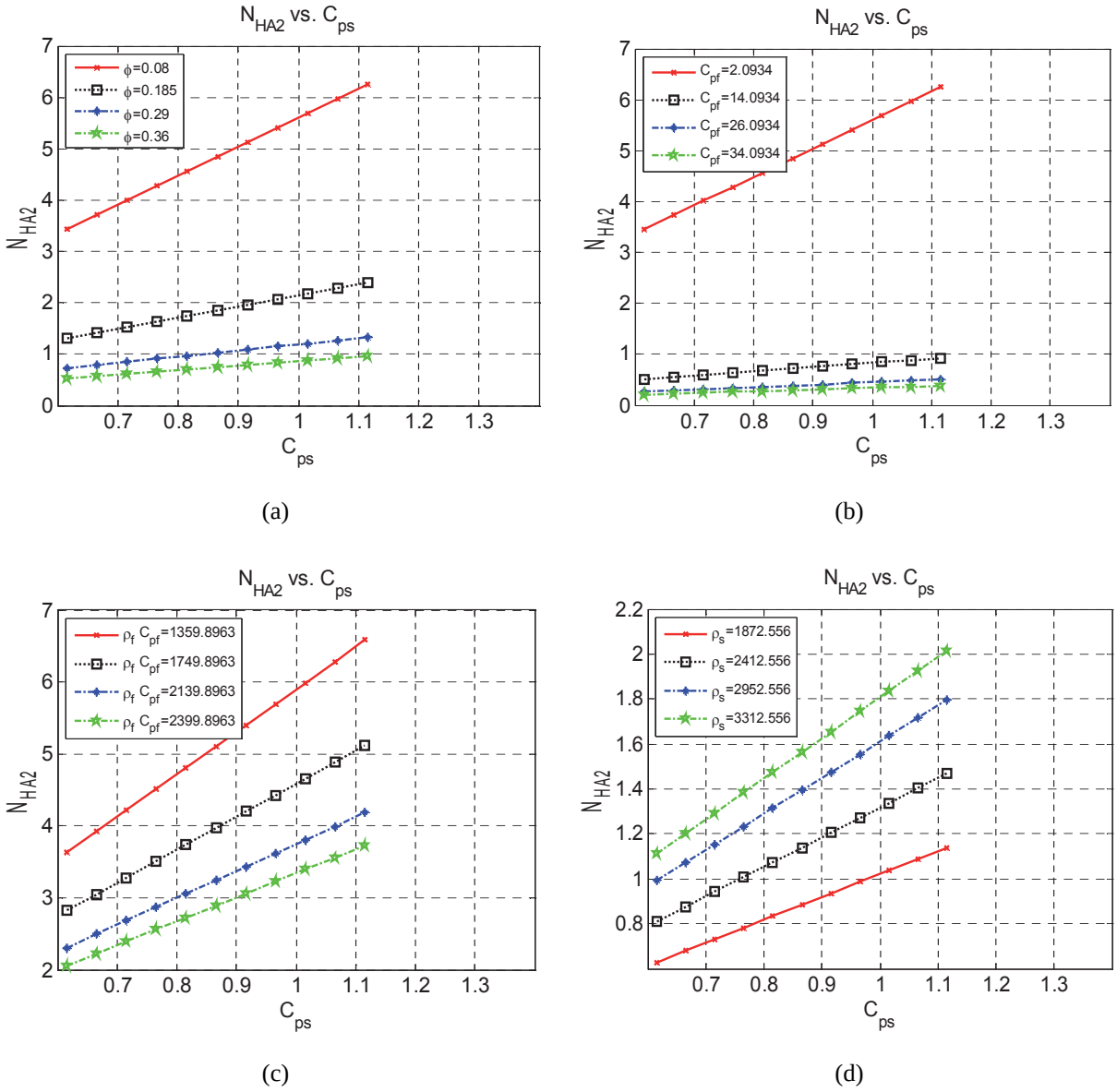

FIG. 8: Variation of (N_{HA2}) with specific heat capacity of solid (c_{ps}) for different porosities (φ), specific heat capacities of fluid (c_{pf}), ($\rho_f c_{pf}$), and rock densities (ρ_s)

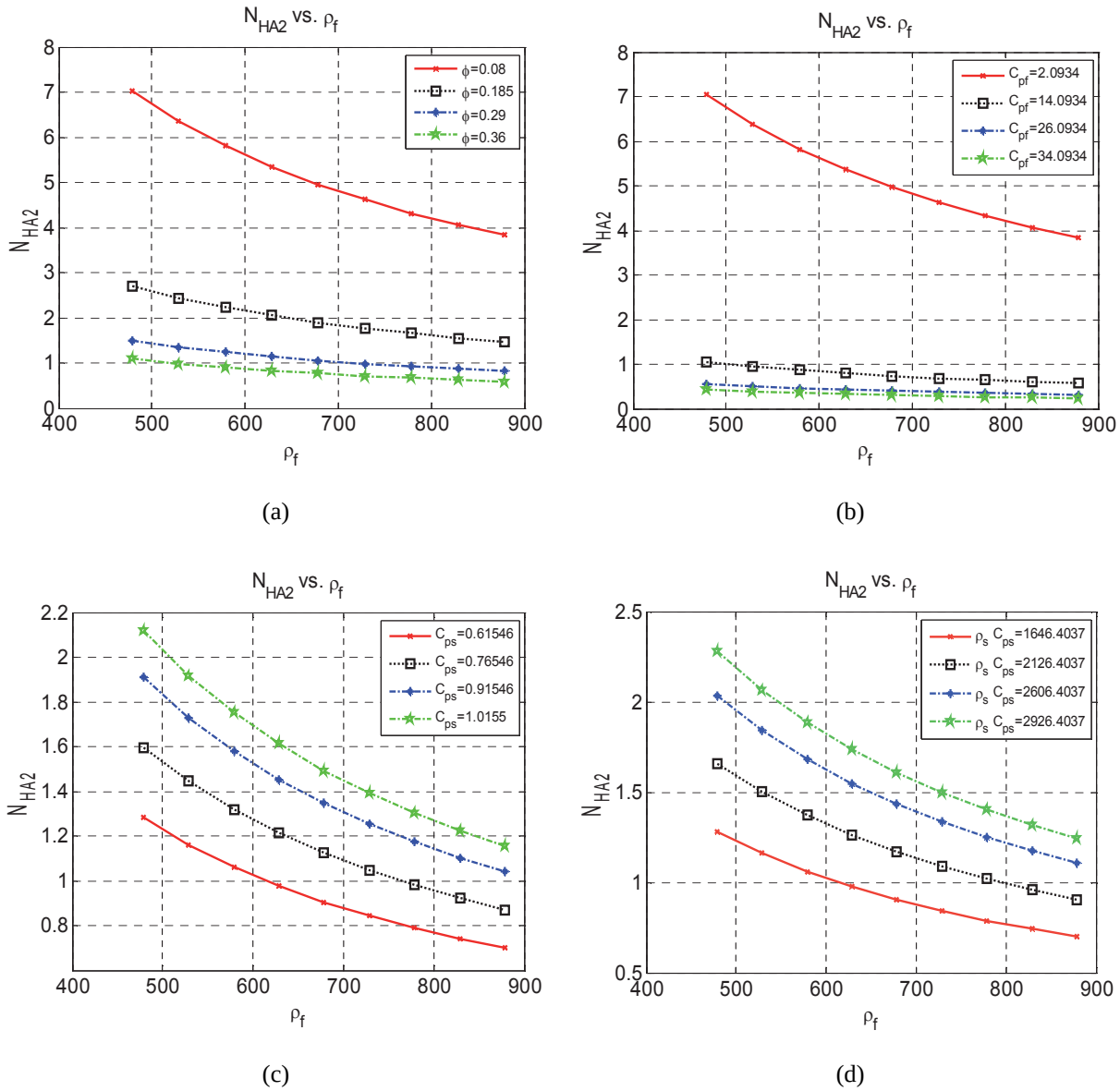

FIG. 9: Variation of (N_{HA2}) with fluid density (ρ_f) for different porosities (φ), specific heat capacities of fluid (c_{pf}), specific heat capacities of solid (c_{ps}), and ($\rho_s c_{ps}$), respectively

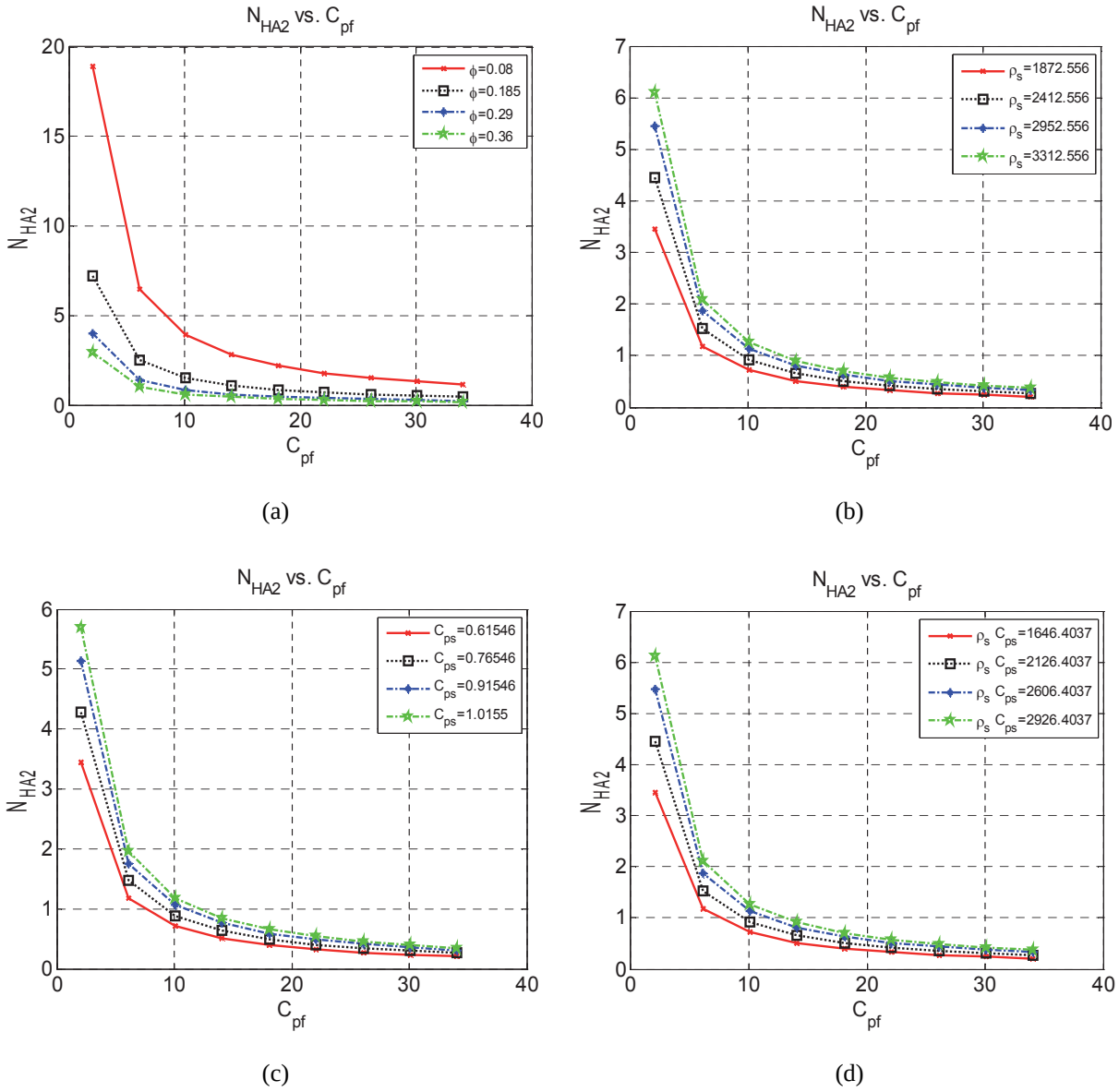

FIG. 10: Variation of (N_{HA2}) with specific heat capacity of fluid (c_{pf}) for different porosities (φ), rock densities (ρ_s), specific heat capacities of solid (c_{ps}), and ($\rho_s c_{ps}$)

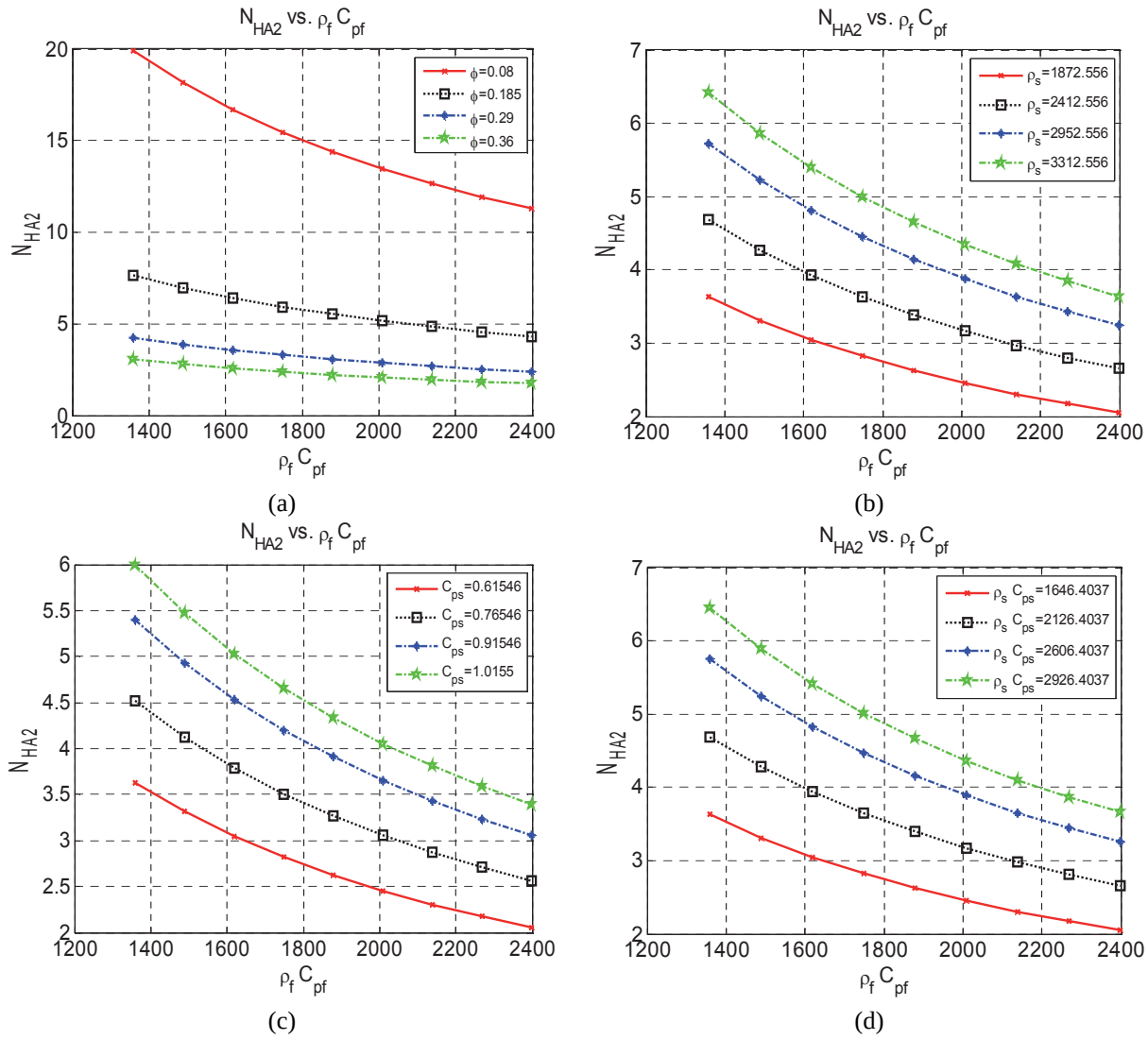

FIG. 11: Variation of (N_{HA2}) with ($\rho_f c_{pf}$) for different porosities (φ), rock densities (ρ_s), specific heat capacities of solid (c_{ps}), and ($\rho_s c_{ps}$)

trends as observed earlier with c_{pf}. The trend and pattern of N_{HA2} versus $\rho_f c_{pf}$ are almost the same for all investigated parameters. However, for the same $\rho_f c_{pf}$ value, N_{HA2} decreases with the increase of φ and increases with the increase of ρ_s, c_{ps}, and $\rho_s c_{ps}$. Thus, N_{HA2} is more sensitive to $\rho_s c_{ps}$ at low porosity as shown in Fig. 11(a).

6. CONCLUSIONS

Mathematical models with the inclusion of the memory concept are presented here to introduce dimensionless numbers that can be useful for characterizing reservoir rock/fluid properties. Formulated for porous media applications, the two proposed dimensionless numbers are capable of handling variable rock and fluid properties with time and space. They are sensitive to rock/fluid rheological properties and can explain such properties if the rock and fluid temperatures are different. The utility of the proposed numbers lies in the ability to characterize the rheological properties of a reservoir if those numbers are known for another analogous reservoir, thus eliminating the need for rigorous investigation.

ACKNOWLEDGMENT

The authors acknowledge the support provided by the Deanship of Scientific Research (DSR) at King Fahd University of Petroleum and Minerals (KFUPM) for funding this work through Project No. JF100009.

REFERENCES

Chan, Y. T. and Banerjee, S., Analysis of transient three-dimensional natural convection in porous media, *J. Heat Transfer*, vol. **103**, pp. 242–248, 1981.

Dawkrajai, P., Lake, L. W., Yoshioka, K., Zhu, D., and Hill, A. D., Detection of water or gas entries in horizontal wells from temperature profiles, *Proc. of SPE/DOE Symposium on Improved Oil Recovery*, Tulsa, OK, April 22–26, SPE-100050, 2006.

Hossain, M. E., An experimental and numerical investigation of memory-based complex rheology and rock/fluid interactions, *Ph.D. dissertation*, Dalhousie University, Halifax, Nova Scotia, Canada, p. 773, 2008.

Hossain, M. E. and Islam, M. R., An advanced analysis technique for sustainable petroleum operations, VDM Verlag Dr. Muller Aktiengesellschaft & Co. KG, Saarbrücken, Germany, p. 655, 2009.

Hossain, M. E., Abu-Khamsin, S. A., and Al-Helali, A., Use of the memory concept to investigate the temperature profile during a thermal EOR process, SPE - 149094, presented at the 2011 SPE Saudi Arabia Section Technical Symposium and Exhibition held in Al-Khobar, Saudi Arabia, 15–18 May, 2011.

Hossain, M. E., Mousavizadegan, S. H., Ketata, C., and Islam, M. R., A novel memory based stress-strain model for reservoir characterization, *J. Nat. Sci. Sustainable Technol*., vol. **1**, no. 4, pp. 653–678, 2007.

Hossain, M. E., Mousavizadegan, S. H., and Islam, M. R., The effects of thermal alterations on formation permeability and porosity, *Pet. Sci. Technol*., vol. **26**, no. 10-11, pp. 1282–1302, 2008a.

Hossain, M. E., Mousavizadegan, S. H., and Islam, M. R., Rock and fluid temperature changes during thermal operations in EOR processes, *J. Nat. Sci. Sustainable Technol*., vol. **2**, no. 3, pp. 347–378, 2008b.

Hossain, M. E., Mousavizadegan, S. H., and Islam, M. R., A new porous media diffusivity equation with the inclusion of rock and fluid memories, *SPE-114287-MS*, Allen, TX: Society of Petroleum Engineers, 2008c.

Hossain, M. E., Mousavizadegan, S. H., and Islam, M. R., Effects of memory on the complex rock–fluid properties of a reservoir stress–strain model, *Pet. Sci. Technol*., vol. **27**, no. 10, pp. 1109–1123, 2009a.

Hossain, M. E., Mousavizadegan, S. H., and Islam, M. R., Variation of rock and fluid temperature during thermal operations in porous media, *Pet. Sci. Technol*., vol. **27**, pp. 597–611, 2009b.

Kaviany, M., *Principles of Heat Transfer*, pp. 885–897, New York: Wiley, 2002.

Marx, J. W. and Langenheim, R. H., Reservoir heating by hot fluid injection, *Trans. AIME*, vol. **216**, pp. 312–315, 1959.

Spillette, A. G., Heat transfer during hot fluid injection into an oil reservoir, *J. Can. Pet. Technol*., vol. **4**, no. 4, pp. 213–218, 1965.

Willman, B. T., Valleroy, V. V., Runberg, G. W., Cornelius, A. J., and Powers, L. W., Laboratory studies of oil recovery by steam injection, *J. Pet. Technol*., vol. **13**, no. 7, pp. 681–690, 1961.

Yoshioka, K., Zhu, D., Hill, A. D., and Lake, L. W., Interpretation of temperature and pressure profiles measured in multilateral wells equipped with intelligent completions, *Proc. of SPE Europec/EAGE Annual Conference*, Madrid, Spain, June 13–16, SPE-94097, 2005a.

Yoshioka, K., Zhu, D., Hill, A. D., Dawkrajai, P., and Lake, L. W., A comprehensive model of temperature behavior in a horizontal well, *Proc. of SPE Annual Technical Conference and Exhibition*, Dallas, TX, October 9–12, SPE-95656, 2005b.

Yoshioka, K., Zhu, D., Hill, A. D., Dawkrajai, P., and Lake, L. W., Detection of water or gas entries in horizontal wells from temperature profiles, *Proc. of SPE Europe/EAGE Annual Conference and Exhibition*, Vienna, Austria, June 12–15, SPE-100209, 2006.